Geophys. J. Int. (1994) **118,** 47–56

Numerical simulation of high- and low-frequency *Lg*-wave propagation

Richard L. Gibson, Jr[1,*] and Michel Campillo[2]

[1] *Earth Resources Laboratory, Department of Earth, Atmospheric and Planetary Sciences, Massachusetts Institute of Technology, Cambridge, MA 02139, USA*

[2] *Université Joseph Fourier, IRIGM—BP 53X, 38041 Grenoble, France*

Accepted 1993 December 22. Received 1993 December 22, in original form 1993 May 31

SUMMARY

Lg waves are sometimes extinguished when traversing geological structures such as mountain ranges or grabens. Previous investigations have applied numerical, full-waveform simulations at relatively low frequencies (on the order of 1 Hz) to investigate the relationship of different structural models and the amplitude anomalies of the *Lg* waves. These studies often fail to link specific known structures to the amplitude anomalies. However, the observed waveforms also often contain data of significantly higher frequency than the full waveform simulations. We compare such low-frequency simulations computed with the boundary-integral-equation (BIE) technique with synthetic seismograms generated by dynamic ray tracing (DRT). Beginning with a plane-layered model of the crust in central France, we show that the general characteristics of the *Lg* wave train over distances ranging from 100 km to around 500 km can be modelled by computing a relatively small number of rays reflected between the free surface and the Moho. Matching the details of the waveforms is more difficult, but can be improved by the addition of reflections between other interfaces in the model. Considering a one-layer model of the crust with a step-like change in Moho depth that leads to a rapid decrease in crustal thickness, we show again that the BIE and DRT solutions are very similar in character. Significantly, both solutions predict that the *Lg* wave will not be extinguished on traversing the Moho step. Finally, we consider a more complete and detailed model of the Pyrénées. Though it is more difficult to match exactly the ray- and integral-equation solutions, the general trends continue to be the same, and the *Lg* waves are still predicted to cross the tectonic structures associated with the mountains. Therefore, it appears that observed amplitude changes must be caused by something other than the general structure of the Pyrénées, such as scattering by smaller scale features within the lower crust.

Key words: boundary-integral-equation methods, *Lg* waves, ray tracing, seismic modelling, synthetic seismograms.

INTRODUCTION

The dominant signals observed at regional distances, from about 150 km to several thousand kilometres, are the *Pg* and *Lg* waves (Campillo 1987). In particular, the *Lg* waves are composed of shear-wave energy that is trapped in the crust and hence can be considered to be shear waves reflected post-critically between the free surface and the Moho (Bouchon 1982; Olsen, Braile & Stewart 1983). This wave generally shows a strong signal that has often proved useful in estimating nuclear yields (e.g. Hansen, Ringdal & Richards 1990; Nuttli 1988). At the same time, early investigations demonstrated that the existence of an oceanic segment of the travel path between the source event and the observation location will tend to extinguish the *Lg* wave (Press & Ewing 1952). Likewise, the wave propagation often shows anomalous extinction of the *Lg* waves when the

* Formerly: Université Joseph Fourier, IRIGM—BP 53X, 38041 Grenoble, France.

travel path traverses geological structures such as grabens or mountain ranges (Ruzaikin *et al.* 1977; Kennett *et al.* 1985; Campillo *et al.* 1993). It is often difficult to explain these extinctions in terms of relatively well-known geological structural models, as the computation of synthetic seismograms using these models predicts that the *Lg* waves should propagate with a much smaller degree of amplitude reduction than is observed.

Numerical synthesis of *Lg* waveforms has generally focused on the application of full-waveform methods, such as discrete wavenumber methods, modal-summation techniques, and the boundary-integral-equation approach (Bouchon 1982; Kennett & Mykkeltveit 1984; Campillo & Bouchon 1985; Campillo 1987; Campillo *et al.* 1993; Chazalon *et al.* 1993). While these solutions are very useful because in principle they can include the effects of all diffractions, reflections and transmissions in the resulting synthetic seismograms, they are also generally limited to relatively low frequencies due to the computation times and computer sizes required for higher frequencies. Likewise, a finite-difference solution might be proposed, but such methods are in general susceptible to significant dispersion errors when simulating wave propagation over distances of hundreds of wavelengths (Fornberg 1987; Sei 1993). The accuracy of this approach might therefore also be questioned for higher frequencies and large distances. In contrast, ray methods provide a high-frequency asymptotic solution to the wave equation, which can yield synthetic seismograms with a much more rapid computation time. This can be useful when the observed data contain frequencies higher than those that can be used in the full-waveform solutions. Kennett (1986) has used some ray calculations to obtain some intuitive understanding of the effects of geological structure on *Lg* waves by computing ray paths and plotting reflection points (see also Bostock & Kennett 1990; Kennett, Bostock & Xie 1990). This method demonstrates the influence of Moho and crustal geometry on focusing and defocusing of seismic waves.

Because of the approximate nature of the ray solution, however, there are certain fundamental limitations that must be recalled if the method is to be applied to synthesize the *Lg* waveforms. Most importantly, aspects of wave propagation such as diffraction cannot be considered, and an explicit description of all ray reflections of interest is required. Another practical consideration is that features such as velocity gradients and curved interfaces will lead to caustic surfaces in the wavefields, which will have unrealistically high amplitudes in the ray approximation. In application to the problem of *Lg*-wave propagation, we can therefore anticipate some difficulties for complicated models with curved interfaces corresponding to an irregular Moho or other features.

In this paper, we use the dynamic-ray-tracing (DRT) method (Červený 1985) to synthesize the *Lg* waves and compare the results with full waveform calculations from the boundary-integral-equation (BIE) algorithm. The basic point that we want to address is to prove that the frequency domains of applicability of the two approaches overlap for the crustal models that we consider here, and that as long as a sufficient number of ray paths is considered, ray theory can be used to simulate *Lg* wave propagation in the high-frequency limit. We describe briefly both of these numerical methods, along with a simple algorithm for automatically detecting the caustics created by curved interfaces and rejecting rays that are on the caustic surfaces in order to calculate synthetic seismograms with reliable amplitude information. Beginning with a simple plane-layered model of the crust of central France, we then show that the two approaches give very similar results and that only a few post-critical reflections need be computed using the ray method to obtain a good estimate of the leading order trends of the *Lg* wave. We continue by examining a simple one-layer model with an irregular Moho and show that again the methods of the two approaches are similar. Finally, we consider a realistic model of the Pyrénées mountains and show that both the BIE and the DRT solution predict that the *Lg* wave should propagate across the mountain range relatively unattenuated. This is in contrast to the observed extinction of the waves (Chazalon *et al.* 1993).

METHODS

Boundary integral equation

Boundary integral equations can be used to compute the elastic response in a very broad class of problems. The classical direct boundary integral equation technique has been used extensively in engineering to solve diffraction problems (see, for example, Brebbia 1978). The indirect BIE technique is based on the integral representation of diffracted fields by the radiation of distributions of sources along the boundaries. This approach allows a rather simple physical interpretation in terms of Huygen's principle. The unknown source distributions are found by matching the boundary conditions at each interface in the model. The discretization of the problem can be done by integration of the Green function along small elements of the boundary (e.g. Sanchez-Sesma & Campillo 1991). An alternative approach consists of the use of the discrete wavenumber representation of the Green's function (Bouchon 1985; Campillo & Bouchon 1985). In this context, the well-known singularity problem of the Green's function is avoided by using truncated series in place of actual Green's functions. This technique has been shown to give very accurate results in different applications (Campillo 1987; Bouchon & Schmitt 1989; Axilrod & Ferguson 1990; Liu & Randall 1991). It can be extended to the case of multilayered media having irregular interfaces (Bouchon, Campillo & Gaffet 1989). While we do not expect a degradation of the solution at high frequency, this technique is limited to the domain of the low frequencies because of its requirement of large computation time when the ratio of model dimension to wavelength becomes too large.

In application to the problem of regional wave propagation, we can use the BIE technique for frequencies up to 1 Hz. At higher frequencies, and in absence of further limitations, the computation becomes extremely time intensive, especially because of the very large size of the matrices which must be inverted (Bouchon *et al.* 1989). When we compare short-period regional data with synthetics, we may suggest that the propagation properties deduced from simulations at frequencies less than or equal to 1 Hz cannot be extrapolated to waves with higher

frequencies. This motivates a comparison of the BIE solution with another approach that is computationally more feasible at high frequencies.

Dynamic ray tracing

Ray-tracing equations

The ray method is based on a high-frequency asymptotic solution to the wave equation (Karal & Keller 1959; Červený, Molotov & Pšenčík 1977; Aki & Richards 1980; Ben-Menahem & Singh 1981; Červený 1985; Ben-Menahem & Beydoun 1985). Application of ray solutions is therefore limited to media where the scale length of the heterogeneity is much longer than a wavelength (Ben-Menahem & Beydoun 1985). For a weakly inhomogeneous, isotropic and elastic medium, the following system of first-order differential equations is obtained (e.g. Červený 1985):

$$\frac{dx_i}{d\tau} = v^2 p_i$$
$$\frac{dp_i}{d\tau} = -\frac{1}{v}\frac{\partial v}{\partial x_i}, \tag{1}$$

where x_i is the Cartesian coordinate, p_i is the coordinate of the slowness vector, v is either the P-wave velocity α or S-wave velocity β, and τ is traveltime. Integration of this system of equations yields the ray path and the traveltime along the ray. Eq. (1) thus determines the kinematic aspects of the wave propagation from source to a far-field observation point.

In order to obtain ray amplitudes, however, further information is needed. This can be accomplished via DRT, which involves calculation of the local wavefront curvature. Utilization of ray-centred coordinates results in a particularly rapid algorithm. The ray-centred coordinates q_i, are a local coordinate system on the ray with three mutually perpendicular basis vectors, one of which is defined to be tangent to the ray (Popov & Pšenčík 1978; Červený & Hron 1980; Červený 1985). In these coordinates, the following equations are integrated

$$Q_{IJ} = v^2 P_{IJ}$$
$$P_{IJ} = -\frac{1}{v}\frac{\partial^2 v}{\partial x_i \partial x_j} Q_{IJ}. \tag{2}$$

In these expressions, $I, J = 1, 2$. The geometrical spreading contribution to the amplitude is directly related to the determinant of $\mathbf{Q}$ (Červený 1985). When reflection and transmission coefficients are calculated at each point where the ray encounters an interface within the model, the amplitude of the wave arriving at a receiver is then known. The effect of the source-radiation pattern on the amplitude is also easily incorporated into the calculations using the expressions given by Ben-Menahem, Gibson & Sena (1991), who demonstrate that in a general elastic medium, the far-field, high-frequency radiation pattern is obtainable using only quantities that are known from the DRT. Note also that the initial values of these matrices can be set to model either a point source or a line source in a given earth model (Červený 1985).

The matrices $\mathbf{P}$ and $\mathbf{Q}$ used to compute geometrical spreading are also necessary for the application of the paraxial method. Because the product

$$M_{IJ} = P_{IK}(Q^{-1})_{KJ} = \frac{\partial^2 \tau}{\partial q_I \partial q_J} \tag{3}$$

yields the second derivatives of the traveltime near the ray, it can be used to estimate the traveltime at a receiver that is close to the ray (Červený 1985; Červený, Klimes & Pšenčík 1984). Similar types of equations can be obtained for corrections to polarization at the receiver. Use of this paraxial method then significantly simplifies the ray tracing, since the ray need only arrive near the receiver point. Some conditions for the validity of the method relating the distance between ray and receiver to such parameters as wavelength and characteristic length of the model are discussed by Beydoun & Keho (1987). The typical scale length of the earth model provides an important criterion, since the extrapolation of traveltimes and amplitudes should not be attempted over distances greater than this characteristic length.

Ray tracing for Lg waves

In application to simulations of Lg-wave propagation, some of the more difficult aspects of ray tracing become important. For example, in a simple plane-layered medium, there is a unique ray travelling from source to receiver, reflecting one time from the Moho, but for the 2-D models

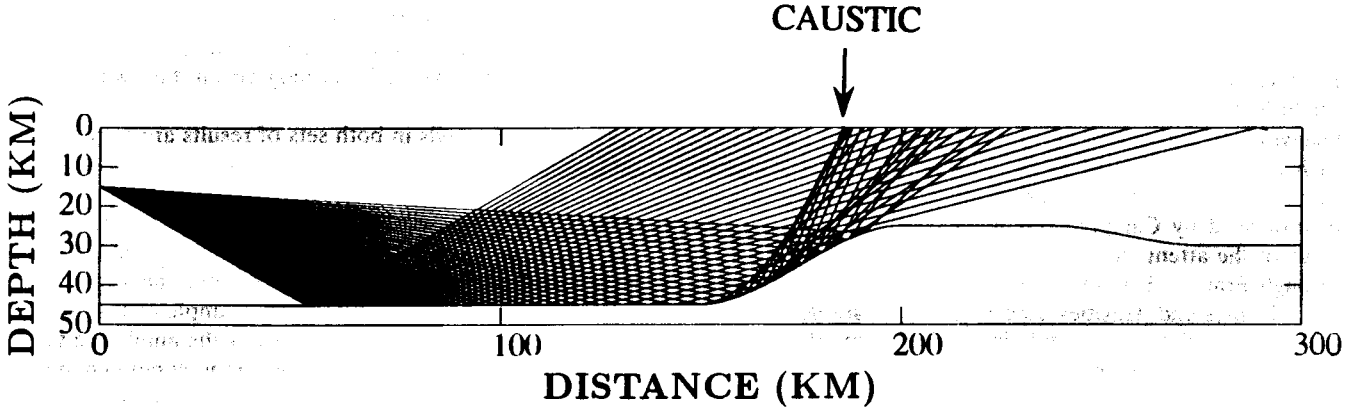

Figure 1. Example of a caustic surface formed by the geometry of irregular Moho surfaces. Ordinarily, the caustic will result in artificially large amplitudes in synthetic seismograms computed by ray techniques. These effects can be minimized using the method described in the text.

considered for this paper, there are in general several such rays for a single source/receiver pair. The ray paths in Fig. 1 illustrate this effect. For some receiver positions, rays will arrive after reflecting from the sloping portion of the interface as well as from the planar region. Normally, when using the paraxial method, the ray arriving closest to the receiver can be used as the basis for extrapolation of time and amplitude information. For models where multiple arrivals occur, however, it is important to consider take-off angle as well as offset of the ray endpoint from the receiver in choosing rays for application of the paraxial correction. If the take-off angles of two rays arriving close to the receiver are sufficiently different, they are in fact distinctly different arrivals and both should be added to the synthetic seismograms.

Another case where the choice of rays is difficult is in regard to the focusing effects of the curved interfaces. As shown in Fig. 1, the locally strong curvature of the interface generates caustics in the reflected wavefield, which can result in artificially high-amplitude calculations for some receiver locations. We can take advantage of the paraxial method to resolve this difficulty. In order to avoid choosing a ray that is located on the caustic, we compute the rate of change in geometrical spreading with take-off angle while doing the ray tracing, and if the change from one ray to the next is extremely large with respect to the actual value of the geometrical spreading, the ray is not used for the paraxial method. Then the ray closest to the receiver, yet not on the caustic will be chosen, and since this ray will have a realistic amplitude, the paraxial corrections can be applied and a much more accurate synthetic seismogram is obtained. Failure to perform this ray selection step with complicated models will cause the synthetic seismograms to contain several isolated, unrealistically large arrivals. These are in general obvious, so that it is straightforward to perform the ray tracing both with and without the ray-selection procedure to be sure that only the unrealistic signals are eliminated. While this intuitive solution to the caustic problem is not completely rigorous in the sense of being derived from first principles, it will lead to synthetic seismograms that are far more accurate than the results obtained by using the ray amplitude at the caustic, which would be found by simply choosing the closest ray.

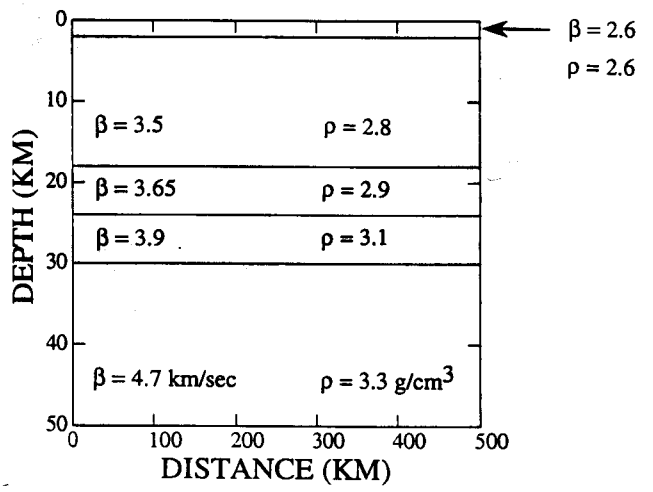

Figure 2. Horizontally layered model of the crust of central France (Perrier & Ruegg 1973). Densities ρ and the shear-wave velocities β are indicated in the figure. Synthetic seismograms computed using this model are presented in Figs 3 and 5.

COMPARISONS OF METHODS

Lg wave in a plane-layered model

By considering first a plane-layered earth model, we can establish the validity of using ray methods to simulate the behaviour of *Lg* waves. Perrier & Ruegg (1973) developed such a four-layer model of the crustal structure of central France based on refraction experiments, a model which was in turn used by Campillo, Plantet & Bouchon (1985) in a study of the attenuation properties of *Lg* waves propagating through France. This model is shown in Fig. 2 along with the velocities and densities used in the calculations.

In this special case, a full implementation of the BIE method is not necessary, as a direct implementation of the discrete wavenumber numerical solution, along with propagator-matrix methods, can be used to compute the full wavefields. The code we use for this utilizes a point source and computes the fully 3-D geometrical spreading. Results for the calculation of the *SH*-wave response of the model by this method are presented in Fig. 3(a). A Ricker wavelet with a central frequency of 1 Hz was convolved with the computed impulse response, and each trace is multiplied by a gain factor of $r^{2/3}$, where r is epicentral distance from source to receiver. The source, a double couple oriented to produce only *SH* waves in the direction of the receiver array, was located at a depth of 10 km. The corresponding DRT results are shown in Fig. 3(b), where a number of rays have been computed for comparison with the BIE results. Specifically, we computed the rays reflected between Moho and the free surface up to 10 times, the ray travelling directly from the source to each receiver, and the rays reflected in the shallowest 2.0 km thick crustal layer between the free surface and the first interface. Additionally, we calculated the rays reflecting up to 10 times between each of the other interfaces and the free surface, and several combinations of rays reflecting from several different interfaces. Because these latter rays do not reflect post-critically from the Moho, their contribution to the overall synthetic seismogram is comparatively minor. The ray-theoretical seismograms were scaled in the same way as were the results from the BIE method, so the relative amplitudes of the synthetic seismograms in the two plots are directly comparable.

The general trends in both sets of results are very similar. The dominant arrivals consist of pairs of post-critically reflected *SH* waves, where the first arrival within each pair is the wave travelling downwards from the source position to reflect first from the Moho, and the second is the wave that first travels upwards to reflect once from the free surface before impinging on the Moho. An example of thse pairs is marked in Fig. 3(a). In Fig. 4, we show the amplitude versus offset curves of one of these reflections computed by ray tracing. The mode-like behaviour of these trapped, post-critically reflected waves is apparent, in that as distance becomes greater, more and more reflections contribute to

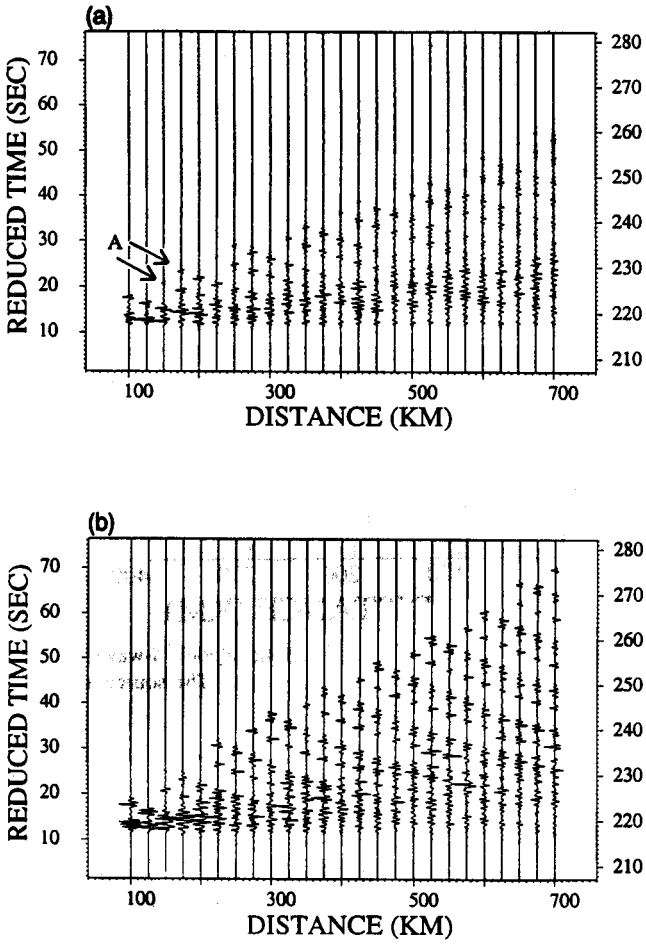

Figure 3. Synthetic seismograms computed using the horizontally layered model in Fig. 2 with a Ricker wavelet of centre frequency 1 Hz. The letter A in each section marks a pair of arrivals, the first of which leaves the source point in the downwards direction. The second arrival initially travels upwards towards the free surface. After leaving the source, both rays reflect twice from the Moho before arriving at the receiver point. The plot was prepared with a reduced traveltime, using the reduction velocity of 3.5 km s^{-1}, but the time axes are labelled to indicate the true arrival time at the distances represented by the axes (i.e. 40 and 760 km). (a) Results of the BIE method. (b) Results of the DRT method.

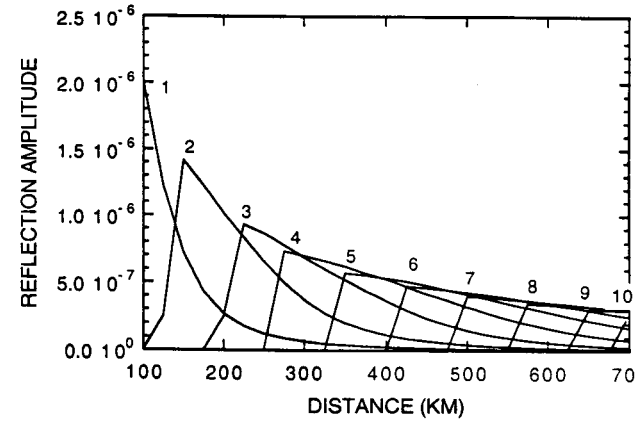

Figure 4. Amplitude versus offset curves for *SH* waves reflected between the free surface and the Moho. The ray reflects first from the Moho. In this figure, the digits indicate the number of reflection points on the Moho. Thus, it is apparent that a distance from the source increases, so does the number of post-critically reflected *SH* waves contributing to the seismogram.

the synthetic seismograms with significant amplitudes. Conversely, this also demonstrates that only a fairly limited number of post-critically reflected *SH* waves need be computed to simulate the dominate reflections in the *Lg* wave train.

While the ray method can simulate the *Lg* waves fairly well, there are still some consistent differences between the two sets of results. First, there are additional small arrivals present in the BIE result that are absent in the ray results. This low-level energy is due to the additional reflections between the free surface and the various intermediate interfaces in the model and between the different subsurface interfaces. These arrivals are especially strong in the earlier portions of the wave trains, creating a band of energy in the seismograms that corresponds to the arrival of many arrivals at the receiver in the small time period. While some of this energy is missing in the DRT synthetics, this is not a serious limitation on the results, as the larger amplitude arrivals are all accounted for. In principle, the rays corresponding to the small missing arrivals could be computed.

The second difference between the BIE and DRT results is somewhat more subtle. A close comparison of the synthetic seismograms shows that each of the post-critical reflections from the Moho is first seen on the ray computations about one trace, 25 km, closer to the source than for the full waveform solution. The end result is that the *Lg* wave train on the ray synthetic occupies a larger time window at large offsets than does the corresponding signal on the BIE result. This is likely a consequence of the frequency independence of the ray-theoretical solution, which assumes a high frequency of wave propagation. Comparison of the two solutions at a frequency of 5 Hz instead of 1 Hz helps to confirm this suggestion (Fig. 5). For this small increase in frequency, some important changes are seen. The post-critical reflections become important at shorter epicentral distances (compare Figs 3a and 5a), and the results are much more similar to the DRT synthetic seismogram. Therefore, we conclude that the ray method is capable of reproducing the most important properties of *Lg* wave propagation at high frequencies.

Irregular Moho model

The second example we consider is a single-layer crust with an irregular Moho (Fig. 6). A variation of crustal thickness is introduced through a ramp in the Moho, with a linear change in Moho depth of 15 km extending over a horizontal distance of 40 km. The crustal *S*-wave velocity is 3.5 km s^{-1}, and the mantle *S*-wave velocity is 4.7 km s^{-1}.

Synthetic seismograms computed with the BIE method are shown in Fig. 7(a) for a range of offsets from 100 km to 350 km. The source is located at a depth of 10 km, and the distance between receivers is 7.14 km. This source again was defined to be a double-couple source oriented to produce only *SH*-wave radiation. The calculations here are 2-D. As

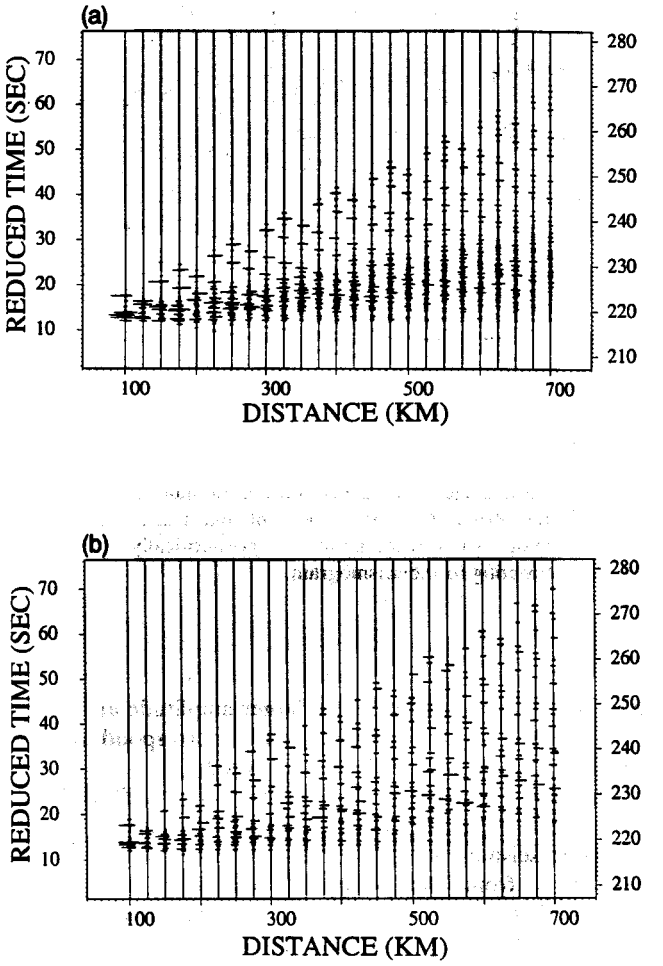

Figure 5. Synthetic seismograms computed using the horizontally layered model in Fig. 2 with a Ricker wavelet of centre frequency 5 Hz. By comparing these results with the 1 Hz synthetic seismograms in Fig. 3, the significant effects of higher frequencies can be observed. It is especially important that at large distances, more post-critical reflections contribute to the BIE synthetic seismogram at 5 Hz than at 1 Hz, so that the *Lg*-wave train is about 10 s longer. The ray synthetic shows the extreme case of this high-frequency behaviour due to the asymptotic nature of this solution. (a) Results of the BIE method. (b) Results of the DRT method.

noted in Fig. 6, the source is located 125 km from the lower corner of the ramp so that the *Lg* waves for this receiver array will be affected by it. The Ricker wavelet has a central frequency of 0.50 Hz. Just as was observed with the plane-layered model, the *Lg* wave consists of pairs of *SH* waves post-critically reflected from the Moho and from the free surface. The general character of the seismograms is much simpler than for the multilayered crust due to the lack of reverberations between the various interfaces.

DRT results for the same source/receiver configuration are very similar in character to the results of the full-waveform calculations (Fig. 7b). A line source, which will result in 2-D geometrical spreading, was utilized to provide results comparable to those obtained with the BIE approach. The same pairs of reflected *SH* waves are seen in the resulting synthetic seismograms, with large amplitudes at

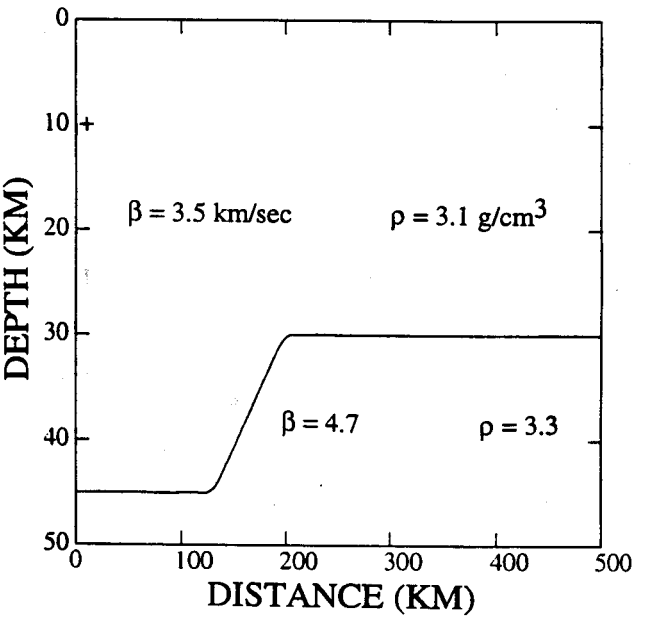

Figure 6. A one-layered, irregular Moho model. *S*-wave velocities β and densities ρ are indicated in the figure. The source location is indicated by a plus symbol.

much the same offsets as for the low-frequency results. The ramp is seen to cause complex interactions of multiple arrivals in each pair as well. For example, at around 200 km from the source, the first pair of *SH*-wave reflections corresponding to one reflection from the Moho (marked A in Fig. 7), abruptly decreases in amplitude. It should be noted that if special care were not taken to eliminate spurious amplitudes from caustics as described above, the synthetic seismograms would contain several unrealistically large-amplitude arrivals due to the caustics generated by the ramp (see Fig. 1).

Some slight differences in the two sets of synthetics again result from the idealized, high-frequency nature of the ray solution. Since the DRT computations cannot include diffractions or scattering from the corners of the ramp, some of the arrivals will terminate more abruptly in the ray results than for the BIE solution (point B in Fig. 7, for example). In addition, the ray results will show the effects of the post-critical reflections at offsets slightly closer to the source than the low-frequency full-waveform results just as in the plane-layered model. However, it is clear that the two methods show essentially the same solution, and that the simple Moho ramp structure has only a small effect on the *Lg* wave, which continues to propagate with only slight complications.

Pyrénéan crustal model

The final model we examine combines the complexities of the plane-layered and Moho ramp models. A representative model of the crustal structure of the Pyrénées mountains along the border between France and Spain includes an irregular Moho as well as multiple layers (Fig. 8) (Chazalon *et al.* 1993). While the upper portion of the crust is principally horizontal, a velocity anomaly is located along

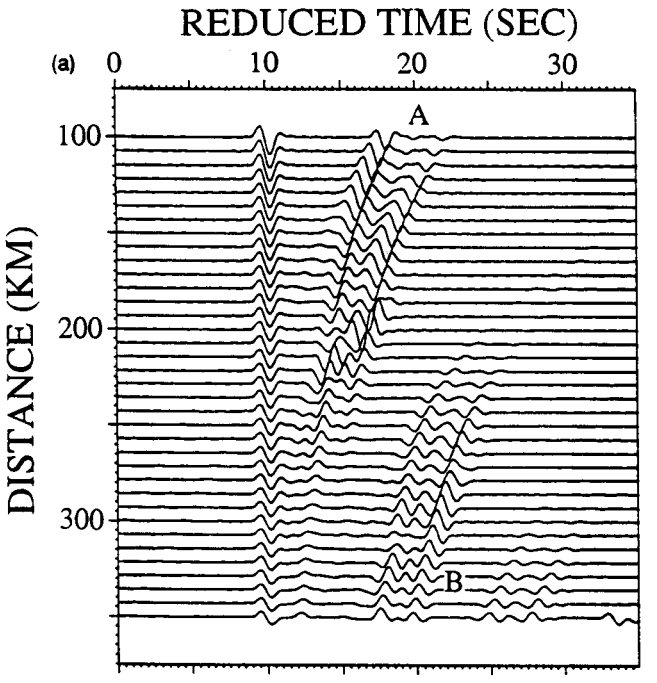

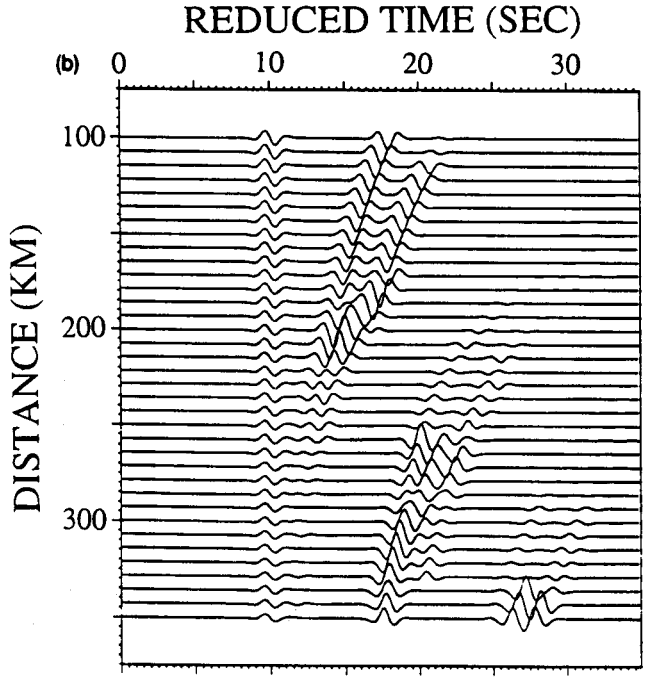

Figure 7. Synthetic seismograms computed from the irregular Moho model in Fig. 6, showing that the full waveform and ray solutions give very similar results. The letter A marks the pair of waves reflected once from the Moho, and B indicates a point where a ray-solution arrival looses amplitude more abruptly than the BIE solution. (a) BIE solution. (b) DRT solution.

the axis of the mountain structure, overlying the ramp in the Moho. A high-velocity region in the lowermost crust is also located over the Moho step. Velocities and densities are indicated in Fig. 8.

This Pyrénéan model is of particular interest due to the

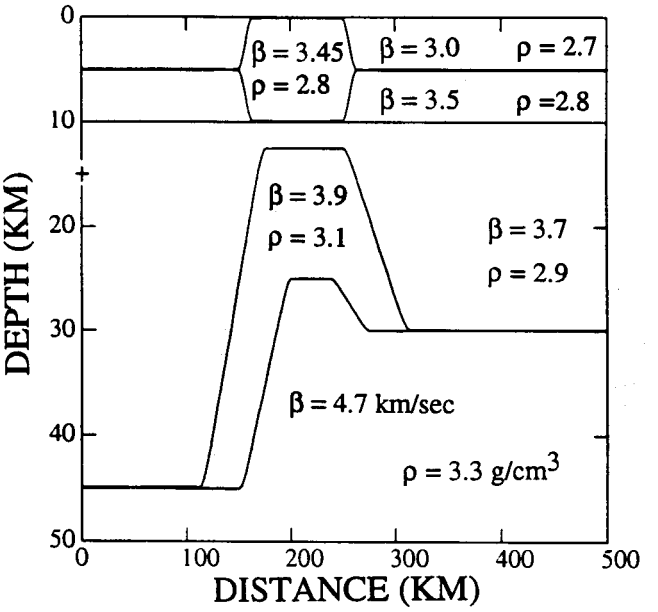

Figure 8. Model of the Pyrénées mountain structure between France and Spain. Shear-wave velocities and densities are indicated in this figure. The source location is indicated by a plus symbol.

anomalous extinction of *Lg* waves that has been observed for some parts of this mountain range. Chazalon *et al.* (1993) performed a detailed study of *Lg* waves propagating both within the crust of Spain and across the Pyrénées structure from Spain to France. After compensating amplitudes for geometrical spreading and attenuation, they carefully compared the waveforms traversing the mountain chain at different points along its length from east to west. While the *Lg* waves that crossed the eastern portion of the range had large amplitudes and were essentially unaffected by the structure, the *Lg* waves that traversed the west end of the Pyrénées were extinguished. These and other observations showed that some feature associated with the western end of the mountain range was causing the extinction of the *Lg* waves. This motivates the synthesis of the *Lg* wave with a realistic model of the geologic structure in order to see if the large-scale structure of the mountain range could be causing the vanishing of the *Lg* wave.

Numerical simulation of the *Lg* wave applied an *SH*-wave source located at a depth of 15 km in the model, 150 km from the Moho ramp (Fig. 8). The source was a double-couple line source as in the previous example. Receivers extended from 100 to 355 km at a spacing of 7.5 km, and a Ricker wavelet of frequency 0.50 Hz was applied. The BIE synthetic seismograms for this model are much more complicated than the results for the two simpler cases due to the effects of the new interfaces and velocity anomalies (Fig. 9). At the distances closest to the source, about 100 to 150 km, a direct *SH* wave and a wave reflected within the upper crust are seen (arrivals A and B, respectively, Fig. 9). The arrival B is reflected within the most shallow crustal layer. Only one pair of Moho reflections is easily visible (arrivals C), and the effects of the Moho structure are very strong around 200 km from the source.

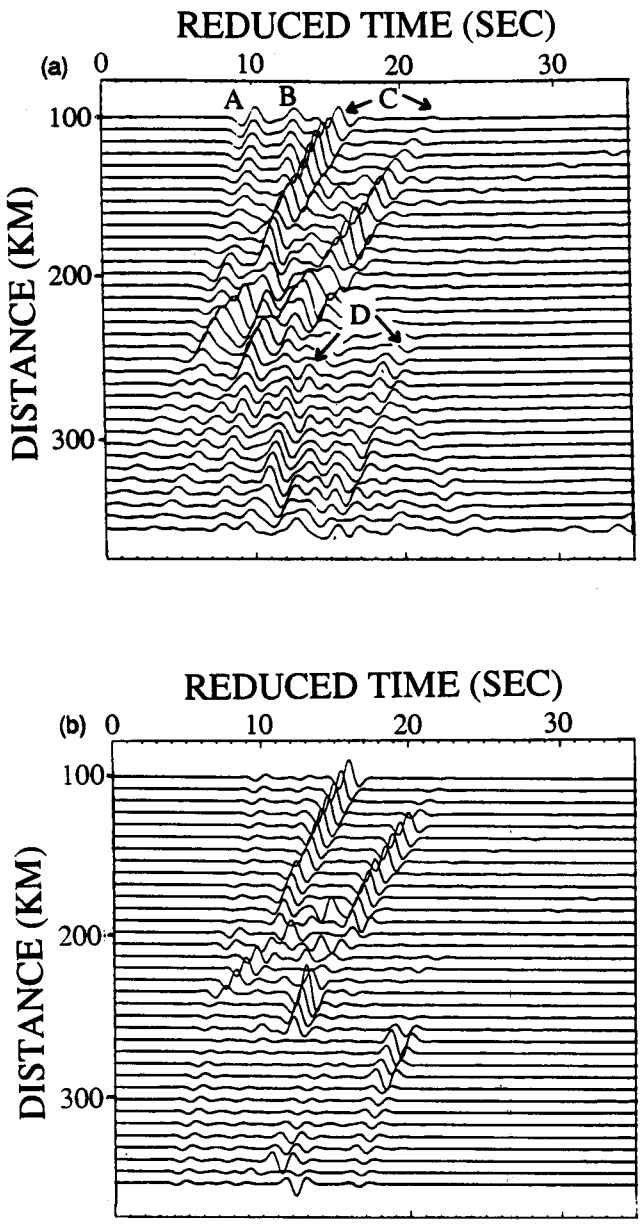

Figure 9. Synthetic seismograms for the Pyrénéan model in Fig. 8. The letters A and B mark the direct *SH* wave and the *SH* wave reflected within the upper crust. C marks the pair of rays reflected between the free surface and Moho one time, and D is a pair of rays reflected twice from the Moho. (a) BIE results, (b) DRT results.

Computations using the BIE method were limited to fairly short offsets for this model due to the complexity of the model. Because the discretization of each irregular interface in the model for the BIE approach requires a significant amount of computer storage, the separation between sources (the periodicity in the space domain) was reduced, and the size of the model and usable receiver offset was reduced. As this problem of computer storage is worse at high frequencies, only very low frequencies could be utilized. Nonetheless, these seismograms in Fig. 9(a) show that there is *Lg*-wave energy that propagates past the complicated mountain range structure at low frequencies, in conflict with the observations of Chazalon *et al.* (1993).

The ray results suffer from other limitations (Fig. 9b). While the high-frequency solution is obtained from this method, it lacks diffractions from the edges and corners in the model, and it is also difficult to account for all possible arrivals. However, the most important trends of the low-frequency BIE solution are retained in the DRT synthetic seismogram (Fig. 9b). Calculations were made using 2-D, line-source conditions. For reasons that are difficult to understand, the relative amplitudes of the arrivals on the receivers nearest the source are mismatched in comparison to the BIE result, but they do show the same changes with offset. Specifically, the waveforms change from a relatively simple to a complicated, incoherent set of arrivals at a distance of around 180 km. In addition, both solutions show a second pair of post-critical *SH* reflections appearing at about 220 km (arrivals D), though the earlier of the two arrivals is slightly weaker in the ray synthetics.

As was true for the other models, there are some other differences in the amplitudes at some offsets resulting from the high-frequency approximation inherent in the ray results, as in the distance at which the post-critical reflection becomes significant. Both methods still agree in showing the propagation of *Lg* waves beyond the structural complexities at high and low frequency. Scattering from small-scale features within the crustal structure under the western end of the mountain chain may instead be the cause of the observed extinction of the *Lg* wave (Chazalon *et al.* 1993).

DISCUSSION AND CONCLUSIONS

We have compared the synthetic seismograms computed by the DRT and BIE methods for three different models, each with differing degrees of complexity. Beginning with a horizontally layered model of the crust of central France, we showed that the two different computational methods give very similar solutions. The principal differences were the lack of some of the waves with very complicated ray paths in the DRT solution and the greater length in time of the *Lg* wave in the ray synthetics at larger distances from the source. This latter effect is caused by the asymptotic, high-frequency nature of the ray solution, which causes the post-critical reflections to have larger amplitudes at slightly smaller offsets. This comparison of results for a simple, 1-D layered model confirms that the ray solution can be used to study *Lg*-wave propagation.

A single degree of complexity was added to the wave-propagation simulations by examining the effects of an irregular Moho in a single layer model of the crust. In this case, the BIE and DRT methods continue to give very similar results, and both predict that the *Lg* wave will propagate beyond the Moho ramp. The amplitudes and waveforms overlying the ramp will be decreased and altered.

Finally, we considered a complicated crustal model of the Pyrénéan mountains between France and Spain. While there are more substantial differences between the results of the two computational methods, the solutions are still qualitatively the same in that they predict an *Lg* wave that propagates past the complicated mountain structure, in contrast to the observed extinction. In addition, both predict very complicated waveforms in the same distance range

overlying the high-velocity zones in the upper and lower crusts.

To make these comments regarding the relative accuracies of the two methods more precise, we consider the amplitude decay predicted by each. In Fig. 10, the maximum amplitude of the synthetic seismograms is plotted as a function of distance. The results for the plane-layered earth model (Fig. 2) are very good, and the reduction in amplitude with offset is the same for both the high-frequency ray calculations and for the BIE results (Fig. 10a). The ray amplitudes show some slight peaks which are not present in the full-waveform solution. These extra peaks are due to the large amplitudes generated at angles of incidence close to the critical angle. Amplitude predictions for the irregular Moho model (Fig. 6) also show some

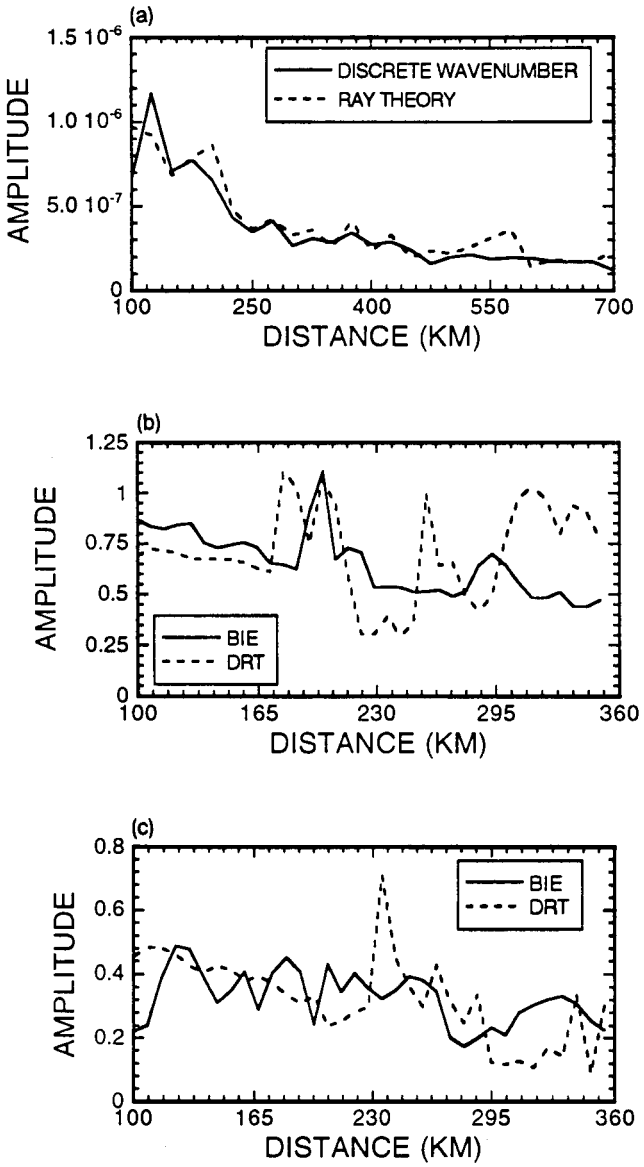

Figure 10. Amplitude as a function of distance predicted for the three earth models in Figs 2, 6 and 8. The curves were obtained by picking the maximum amplitudes of the synthetic-seismogram traces at each offset. (a) Amplitudes for the plane-layered model (Fig. 2). (b) Amplitude predictions for the irregular Moho model (Fig. 6). (c) Amplitudes for the Pyrénéan mountain range model (Fig. 8).

departures that are due mainly to the behaviour of the ray solution near the critical angle (Fig. 10b). In particular, the DRT amplitudes at the largest offsets are larger than the BIE results, but this is due only to the overly large critical ray amplitudes. Calculation of ray amplitudes for larger offsets shows that the amplitude predictions decrease to essentially the same level as the BIE values. The last set of curves, those resulting for the Pyrénéan model (Fig. 8), show the most variation with offset in the BIE solution due to the high degree of structural complexity in the model (Fig. 10c). There are two major differences in the plotted amplitudes. First of all, there is a very high amplitude predicted by the ray method at a distance of 235 km. This amplitude increase is due to focusing by the curvature of the Moho on the side of the bump closest to the source. Likewise, the reason amplitudes tend to be smaller for somewhat larger differences is that the rays are reflecting from a corner on the top of the bump, which tends to exaggerate the decrease in amplitude in the DRT results. However, just as for the other two models, the amplitude predictions from the two methods of computing synthetic seismograms predict essentially the same behaviour with offset.

These results show that the BIE and DRT solutions can both provide insight into *Lg*-wave propagation and that each has its own advantages. Our results have shown that the frequency domains of applicability for these two methods overlap for these models of the crust, thereby suggesting that the conclusions drawn about *Lg*-wave extinction due to the results of low-frequency simulations can in fact be applied to the consideration of high-frequency observations. While the BIE approach yields a full-waveform solution, it is more limited in the size and complexity of the earth models to which it is applied. On the other hand, the DRT method fails to reproduce all aspects of wave propagation, though it does yield the major trends of the *Lg*-wave trains. In addition, the computational speed of the ray method can be a great advantage in application to large source/receiver distances at high frequency and in application to problems that are too large for solution by the BIE method. It is also simple to perform calculations for either a line or a point source simply by changing the initial conditions for the ray equations, allowing a very flexible modelling scheme. Another advantage is that the plotting of ray paths can significantly simplify the identification of individual arrivals and the understanding of the effects of different earth model features on wave propagation. The two methods both have significant value in application to complicated wave-propagation phenomena such as the extinction of *Lg* waves traversing various geological structures.

ACKNOWLEDGMENTS

Comments by Robert Hermann and anonymous reviewer helped to clarify the text and presentation of our results. The first author was supported by Société Nationale Elf Aquitaine (P) through a post-doctoral fellowship at the Université Joseph Fourier, Grenoble, for the initial portions of this work. Additional funding was provided by a Founding Member Post-doctoral fellowship at the Earth Resources Laboratory, Massachusetts Institute of Technology.

REFERENCES

Aki, K. & Richards, P.G., 1980. *Quantitative Seismology*, Vol. 1, Freeman and Company, San Francisco, CA.

Axilrod, H.D. & Ferguson, J.F., 1990. *SH* wave scattering from a sinusoidal grating: an evaluation of four discrete wavenumber methods, *Bull. seism. Soc. Am.*, **80**, 643–655.

Ben-Menahem, A. & Beydoun, W., 1985. Range of validity of seismic ray and beam methods in general inhomogeneous media—I. General theory, *Geophys. J. R. astr. Soc.*, **82**, 207–234.

Ben-Menahem, A. & Singh, S.J., 1981. *Seismic Waves and Sources*, Springer-Verlag, New York.

Ben-Menahem, A., Gibson, Jr, R.L. & Sena, A.G., 1991. Green's tensor and radiation patterns of point sources in general anisotropic inhomogeneous elastic media, *Geophys. J. Int.*, **107**, 297–308.

Beydoun, W.B. & Keho, T.H., 1987. The paraxial ray method, *Geophysics*, **52**, 1639–1653.

Bostock, M.G. & Kennett, B.L.N., 1990. The effect of a 3-D structure on *Lg* propagation patterns, *Geophys. J. Int.*, **101**, 355–365.

Bouchon, M., 1982. The complete synthesis of seismic crustal phases at regional distances, *J. geophys. Res.*, **82**, 1735–1741.

Bouchon, M., 1985. A simple, complete numerical solution to the problem of diffraction of *SH* waves by an irregular interface, *J. acoust. Soc. Am.*, **77**, 1–5.

Bouchon, M. & Schmitt, D., 1989. Full wave acoustic logging in an irregular borehole, *Geophysics*, **54**, 758–765.

Bouchon, M., Campillo, M. & Gaffet, S., 1989. A boundary integral equation-discrete wavenumber representation method to study wave propagation in multilayered media having irregular interfaces, *Geophysics*, **54**, 1134–1140.

Brebbia, C.A., 1987. *The boundary element method for engineers*, Pentech Press, London.

Campillo, M., 1987. *Lg* wave propagation in a laterally varying crust and the distribution of the apparent quality factor in Central France, *J. geophys. Res.*, **92**, 12 604–12 614.

Campillo, M. & Bouchon, M., 1985. Synthetic *SH* seismograms in a laterally varying medium by the discrete wavenumber method, *Geophys. J. R. astr. Soc.*, **83**, 307–317.

Campillo, M., Plantet, J.L. & Bouchon, M., 1985. Frequency dependent attenuation in the crust beneath Central France from *Lg* waves: data analysis and numerical modeling, *Bull. seism. Soc. Am.*, **75**, 1395–1411.

Campillo, M., Feignier, B., Bouchon, M. & Béthoux, N., 1993. Attenuation of crustal waves across the Alpine range, *J. geophys. Res.*, **98**, 1987–1996.

Červený, V., 1985. The application of ray tracing to the propagation of shear waves in complex media, in *Seismic shear waves, Part A: Theory*, ed. Dohr, H.P., in *Handbook of geophysical exploration*, Section 1: Seismic exploration, *15A*, pp. 1–124, eds Helbig, K. & Treitel, S., Geophysical Press, London.

Červený V. & Hron, F., 1980. the ray series method and dynamic ray tracing system for three-dimensional inhomogeneous media, *Bull. seism. Soc. Am.*, **70**, 47–77.

Červený, V., Klimes, L. & Pšenčík, I., 1984. Paraxial ray approximation in the computation of seismic wavefields in inhomogeneous media, *Geophys. J. R. astr. Soc.*, **79**, 89–104.

Červený, V., Molotkov, I.A., & Pšenčík, I., 1977. *Ray methods in seismology*, Charles University Press, Prague.

Chazalon, A., Campillo, M., Gibson, Jr, R.L. & Carreno, E., 1993. Crustal wave propagation anomaly across the Pyrenean range: comparison between observations and numerical simulations, *Geophys. J. Int.*, **115**, 829–838.

Fornberg, B., 1987. The pseudospectral method: comparisons with finite differences for the elastic wave equation, *Geophysics*, **52**, 483–501.

Hansen, R.A., Ringdal, F. & Richards, P.G., 1990. The stability of RMS *Lg* measurements and their potential for accurate estimation of the yields of Soviet underground nuclear explosions, *Bull. seism. Soc. Am.*, **80**, 2106–2126.

Karal, F.C., Jr & Keller, J.B., 1959. Elastic wave propagation in homogeneous and inhomogeneous media, *J. acoust. Soc. Am.*, **31**, 694–705.

Kennett, B.L.N., 1986. *Lg* waves and structural boundaries, *Bull. seism. Soc. Am.*, **76**, 1133–1141.

Kennett, B.L.N. & Mykkeltveit, S., 1984. Guided wave propagation in laterally varying media, II. *Lg* waves in north-western Europe, *Geophys. J. R. astr. Soc.*, **79**, 257–267.

Kennett, B.L.N., Bostock, M.G. & Xie, J.-K., 1990. Guided-wave tracking in 3-D: a tool for interpreting complex regional seismograms, *Bull. seism. Soc. Am.*, **80**, 633–642.

Kennett, B.L.N., Gregersen, S. Mykkeltveit, S. & Newmark, R., 1985. Mapping of crustal heterogeneity in the North Sea basin via the propagation of *Lg* waves, *Geophys. J. R. astr. Soc.*, **83**, 299–306.

Liu, H.L. & Randall, C.J., 1991. Synthetic waveforms in non-circular boreholes using a boundary integral equation method, *61st Annual International Meeting of the Society of Exploration Geophysicists, Expanded Abstracts*, pp. 843–845, Society of Exploration Geophysicists, Tulsa, OK.

Nuttli, O.W., 1988. *Lg* magnitudes and yield estimates for underground Novaya Zemlya nuclear explosions, *Bull. seism. Soc. Am.*, **78**, 873–884.

Olsen, K.H.L., Braile, L.W. & Stewart, J.N., 1983. Modeling short-period crustal phases (*P–Lg*) for long-range refraction profile, *Phys. Earth planet. Inter.*, **31**, 334–347.

Perrier, G. & Ruegg, J.C., 1973. Structure profonde du Massif Central Français, *Ann. Geophys.*, **29**, 435–502.

Popov, M.M. & Pšenčík, I., 1978. Computation of ray amplitudes in inhomogeneous media with covered interfaces, *Stud. Geoph. Geod.*, **22**, 248–258.

Press, F. & Ewing, M., 1952. Two slow surface waves across North America, *Bull. seism. Soc. Am.*, **42**, 219–228.

Ruzaikin, A.I., Neresov, I.L., Khalturin, V.I. & Molnar, P., 1977. Propagation of *Lg* and lateral variations of crustal structure in Asia, *J. geophys. Res.*, **82**, 307–316.

Sanchez-Sesma, F.J. & Campillo, M., 1991. Diffraction of *P*, *SV* and Rayleigh waves by topographic features: a boundary integral formulation, *Bull. seism. Soc. Am.*, **81**, 2234–2253.

Sei, A., 1993. Computational cost of finite-difference elastic waves modeling, *63rd Annual International Meeting of the Society of Exploration Geophysicists, Expanded Abstracts*, pp. 1065–1068, Society of Exploration Geophysicists, Tulsa, OK.